Scientific African 23 (2024) e02029

Contents lists available at ScienceDirect

Scientific African

journal homepage: www.elsevier.com/locate/sciaf

Controlled synthesis and structure characterization of a new fluconazole polymorph using analytical techniques and multivariate method

Bolaji C. Dayo Owoyemi [a,*], Cecilia C.P. da Silva [b], Amos O. Akinyemi [c], Banky O. Amuwaolorun [d], Roxana Lili Roque-Flores [a], Gabriel Lima Barros de Araújo [a], Javier Ellena [b], Renato L. Carneiro [e]

[a] Department of Pharmaceutical Science, University of São Paulo – USP, Av. Professor Lineu Prestes, 580 - Cidade Universitária São Paulo - CEP, SP 05508-000, Brazil
[b] Instituto de Física de São Carlos, Universidade de São Paulo, CEP 369 13.560-970, São Carlos, Brazil
[c] Department of Toxicology & Cancer Biology, University of Kentucky, Lexington, KY 40536, USA
[d] School of Nursing, University of Central Lancashire, Preston PR1 2HE, United Kingdom
[e] Department of Chemistry, Federal University of São Carlos, Rod. Washington Luís km 235, ZIP 13.560-905, São Carlos, SP, Brazil

ARTICLE INFO

Editor: DR B Gyampoh

Keywords:
Fluconazole
Polymorphs
Raman/FT-IR spectroscopy
PCA
XRD
Solubility

ABSTRACT

In the crystallization and search for higher multicomponent forms of fluconazole (FLZ), a metastable FLZ polymorph (concomitant) that manifests in the same crystallization system and transforms into the stable FLZ form (II) after the lyophilization process was observed. In this report, we demonstrated and showed how this FLZ polymorph 10 (*Mw = 306.79 g/mol*) of the monoclinic *C2* space group was detected and reproduced through a controlled lyophilized experiment, and modeled differentiation between vibrational and absorption modes of FLZ functionalities like C=O, OH, $–CH_2$ and –NH. The FLZ polymorph shows strong O–H···N and weak C−H···X (X = N, and F) hydrogen bond and the presence of pi-pi bond interactions in the overlapping triazole rings. The combination of vibrational spectroscopic techniques (Raman/FT-IR) and principal component analysis (PCA) aid the development of important models for polymorph screening and identification. In addition, X-ray diffraction (powder and single crystal) techniques support the polymorph characterization and structure depiction. The PCA models and X-ray diffraction analyses confirmed the newness of FLZ polymorph 10, and further solid-state characterization using thermal techniques (DSC and TGA) affirmed its uniqueness and novelty. Finally, the thermal stability and solubility studies on the new FLZ polymorph were determined to understand its structure properties and compare these with previously reported polymorphs of FLZ.

Introduction

Successful delivery of desired drugs with greater therapeutic potential remains the ultimate priority of all pharmaceutical industries despite the rigorous control of crystallization processes and poor understanding of complexity in intermolecular interactions.

* Corresponding author.
E-mail address: bdayoowoyemi@usp.br (B.C. Dayo Owoyemi).

https://doi.org/10.1016/j.sciaf.2023.e02029
Received 1 April 2023; Received in revised form 7 October 2023; Accepted 19 December 2023
Available online 20 December 2023

Nevertheless, the design and synthesis of *prima materials*, i.e. active pharmaceutical ingredients (APIs), with desired physicochemical and pharmacokinetic properties such as aqueous solubility, bioavailability, and form stability for drug formulations remain vital [1]. However, among the major problems of drug development and formulation is the phenomenon of polymorphism, which is the existence of an API/molecule in different crystalline forms with differences in their physical properties. Interestingly, polymorphism can be explored as a drug optimization approach and has significantly proven to positively aid the optimization of poor drug property issues considering the quantity and uniqueness of crystalline modifications that can exist for a substance. More so, the application and advantages of polymorphism to new drug formulations become fruitless when other polymorphic forms manifest (uncontrolled) during synthesis processes and thus result in variations in drug properties like solubility, dissolution rate, and bioavailability [2–4].

In general, polymorphism is a distinctive property of the crystalline molecular systems (APIs) that results due to lattice arrangements. Therefore, monitoring and controlling cases of polymorphism during crystallization processes and interconversion among polymorphic forms demands a complete understanding of the physicochemical nature of individual drug material. The syntheses and monitoring of polymorphs reported cases of uncontrolled polymorphism in drugs, and interconversion tendencies between polymorphs after the crystallization process were reported in the literature. In addition, reports on the developed analytical techniques for monitoring polymorphic modifications from complex supramolecular synthesis and reproducibility of certain known "disappearing or hidden metastable polymorphs" or concomitants that present desirable/robust properties [5–8].

Fluconazole (FLZ); 2-(2,4-difluorophenyl)-1,3-bis(1H-1,2,4-triazole-1-yl) propan-2-ol), is a slightly soluble multifunction antifungal drug sold Diflucan®. The Biopharmaceutics classification system (BCS) that categorizes drugs based on their solubility and permeability status, classified FLZ as a BSC class II drug. FLZ has the potential to inhibit cryptococcal meningitis by causing damage to yeast and fungal cell membranes. It inhibits cell growth and multiplying, thereby serving as a reliable drug for preventing yeast and fungal infections. FLZ was discovered in 1978, in a research program aimed at the development of a broad-spectrum antifungal agent suitable for the treatment of systemic fungal infections, at Pfizer Central Research in Sandwich, Kent (U.K). Therefore, Richardson and co-workers at the Pfizer Central Research are credited for the discovery of FLZ [9–11]. This antifungal drug exhibits a propensity for polymorphic formation due to its conformational flexibility that can be observed in its functionalities like 2,4-difluorobenzyl, propane skeletal chain attached with a hydroxyl (−OH), and two adjacent triazole groups. However, different stable and metastable polymorphic forms of FLZ with varied physical and pharmacokinetic properties are reported in the literature. Earlier studies reported breakthroughs in the syntheses of FLZ as anhydrous solid forms named I, II (commercialized), and III. Gu and Jiang [12], Yang et al. [13], Dash and Elmquist [14] are the earlier researchers who reported the synthesis of different polymorphic forms of FLZ [15]. In addition, the research work of Alkhamis et al. reported the syntheses of two solvates, a monohydrate, and two anhydrous forms [16]. Recently, the extensive single crystal X-ray diffraction studies reported by Karanam and co-workers contributed by adding four new FLZ polymorphs named; IV, V, VI, and VII [17,18]. Although, FLZ form I (solubility 4.26 mg/mL) and the monohydrate (solubility 3.56 mg/mL) are the most stable forms, both present lower solubility and exhibit slow dissolution rates when compared to the FLZ form II (4.6 and 8 mg/mL) [19–21]. Studies on the polymorphic interconversion between the anhydrate FLZ forms, their hygroscopic tendency, and their transformation into the stable FLZ monohydrate after prolonged exposure at room temperature were reported. In addition, the kinetic solubility and intrinsic dissolution rate (IDR) studies further confirmed that form II presents the highest solubility and IDR. However, its solubility decreases after polymorphic transformation into the more stable FLZ hydrate [22,23].

The physical property challenges of FLZ forms such as low solubility, instability, poor dissolution, and hygroscopicity limit its clinical efficacy and are addressed through different solid state property optimization approaches such as particle size reduction, amorphization, cocrystallization, salt formation, and polymorph design to readdress its efficacy issues. As a complement, this work annexes reports on FLZ multicomponent forms and reveals significant discrepancy (setback) limiting the synthesis of a higher stoichiometric combination of FLZ [20,21,24–26]. In this article, we aim to show the controlled synthesis of a new FLZ polymorph through an effective screening methodology that detects and differentiates this concomitant polymorph that manifests as a "hidden polymorph" after cocrystallization processes. Herein, the decomposition of acquired spectra data (vibrational /absorption modes) of FLZ forms aided the differentiations between the interactions of FLZ functionalities and monitoring the polymorph's reproducible synthesis route using the multivariate method [27].

The principal component analysis (PCA) is a multivariate and pattern recognition technique that uses an orthogonal transformation to reduce higher dimensional data into linearly uncorrelated variables called the principal components (PCs), thereby unveiling latent variations within the decomposed dataset, and indiscriminately presenting their projections in a linear space. As an unbiased and dimensionality-reduction technique, PCA correlates and discriminates between variables using underlying trends and variations that enable the simultaneous visualization of scores and loadings projections for an effective data interpretation [28,29]. Interestingly, the combination of vibrational spectroscopic methods (Raman and FTIR), X-ray diffraction, and PCA are particularly gaining recognition as emerging process analytical tools for material screening, characterization, classification, processes monitoring, and pharmaceutical quality and process control. In this regard, PCA decomposes spectra/diffraction data, amplifies differences in bonds' vibrational energies, and models spectra datasets obtained from Raman and FT-IR vibrational modes [30–33].

In this work, the acquired spectra data (i.e. vibrational modes) of bonded FLZ functionalities and groups like the triazole, 2,4-difluorobenzyl, and hydroxyl (−OH) group attached to the skeletal propane chain in FLZ were selected at spectra range for PCA modeling. This FLZ polymorph was initially observed in the cocrystallization and search for higher multicomponent drug-drug cocrystal forms of fluconazole and Ibuprofen. Herein, the analysis will be performed using organic acids as coformers. The comparatively PCA-Raman and PCA-FT-IR models aid the screening and selection of desired supramolecular synthesis routes for the reproducibility of the new FLZ polymorph. At the same time, the powder XRD analysis provides qualitative identification and confirmation of the differences in crystallinity, phase purity, and robustness of the PCA-assist screened FLZ polymorph. The single crystal X-ray diffraction (SCXRD) unveils the structure of the obtained FLZ polymorph and affirms its novelty. The thermal analysis techniques; differential

scanning calorimeter (DSC) and thermogravimetric analysis (TGA) were employed to determine the material property and detailed thermal events on the homogeneity and stability of the new polymorph. Finally, the experimental determination of its aqueous solubility was performed, calculated, and compared with the previously reported FLZ forms/polymorph.

Experimental section

Materials

The pure FLZ was purchased from Calendula Pharmaceuticals. Coformers; ibuprofen (IBU), adipic (ADP), oxalic (OXL), and malic (MA) acids, purchased from Sigma-Aldrich company at >99 % purity grade. Solvent (HPLC grade); methanol (MeOH), hexanol (Hex), acetonitrile (ACN), and acetone (Ace) were purchased from J.T Bakers Ltd, while the ultra-pure deionized water used is from laboratory fixed MiliQsytem (18.2 mΩ cm).

Supramolecular syntheses

FLZ (30.679 mg, 0.1 mmol) was mixed with each of the coformers; IBU (20.629 mg, 0.1 mmol), ADP (14.614 mg, 0.1 mmol), MA (13.409 mg, 0.1 mmol), and OXL dihydrate (12.606 mg, 0.1 mmol) at 1:1, 1:2, 2:1 stoichiometry ratios and solubilized using different solvent combinations. Note, these *1:1 FLZ/coformer* combinations with these organic acids were reported in our previous reported studies [20,21]. However, a new polymorph was observed as a concomitant in lyophilization reactions (below -4 °C) from these combinations. In this work, the FLZ/MA systems were used to demonstrate spectra screening and PCA data modeling that confirmed the existence of the polymorph.

Fluconazole polymorph synthesis

61.260 mg (0.2 mmol) of FLZ was added to a 10 mL beaker containing a 4 mL solvent mixture of ACN/Ace (v/v, 1:1) and solubilized. The solution was sealed off with an aluminium foil, perforated to lower the rate of solvent evaporation, and was embedded into a 25 mL beaker containing 8 mL of hexanol and sealed off completely using an aluminium foil. The sample was placed inside a refrigerator at a temperature below -4 °C, and crystals suitable for SCXRD analysis were observed after 4 days.

Raman spectroscopy

Raman spectra acquisition was obtained using a B&W Tek BWS 415785H Raman spectrometer (Plainsboro, NJ, USA) coupled to a microscope B&W Tek BAC 151B (Newark, DE, USA). This device has an excitation laser of wavelength 785 nm with a spectral resolution of 3.5 cm^{-1}, 120 s of acquisition time, spectral range of 65–2800 cm^{-1}, laser power of 70 mW, and is managed by BWSpec4.03 software. The equipment aids screening and characterization for evidence of intermolecular interaction by comparing spectra fingerprint region 200–2180 cm^{-1} that incorporate important FLZ functionalities.

Fourier Transform infrared spectrophotometer (FT-IR)

The spectra were obtained from a Shimadzu IRprestige-21 FT-IR spectrophotometer (Kyoto, Japan) managed by Bruker software. Using the potassium bromide (KBr) pallet technique, the equipment was adjusted to take 64 scans, and spectra acquisition was recorded for a wavenumber range from 4000 to 400 cm^{-1} with a resolution of 4 cm^{-1} after the background scan was performed. Spectra comparison at specific regions provides information on new chemical bonds and changes in existing bonds.

Statistical tools

Chemometric computations were performed using Matlab R2011a (Mathworks, Inc., Natick, MA, USA) and the PLS Toolbox 52 (Eigenvector Research, Inc., Manson, WA, USA). OriginLab software Pro9 and Excel software are used to plot/organize raw Raman and FT-IR spectroscopic data, and XRD data into the Matlab R2011a/PLS toolbox.

Principal component analysis (Data pre-processing)

The PCA tool in the PLS toolbox 52 of Eigenvector software in Matlab R2011a was employed to decompose and transform Raman, FTIR, and XRD data into orthogonal factors (principal components) after pre-treatment methods to achieve satisfactory discriminations/correlations between samples. The Raman spectra data (65–2800 cm^{-1}), and FT-IR spectra data (4000–400 cm^{-1}) were loaded and preprocessing was achieved using different algorithms combinations such as Savitzky-Golay first derivative, normalization, and mean centering to remove extraneous variation. The data is linearized to fit the PCA model that adequately presents optimized variations.

X-ray powder diffraction (PXRD)

The X-ray diffraction studies of partially mild crystal powder were performed on a Multiplex X-ray diffractometer (Rigaku

Corporation, Tokyo, Japan), using a copper (Cu) kα radiation (1.54 Å), and a voltage of 40 kV and current of 30 mA. The samples were scanned from 5° to 45° (2θ), at a step size of 0.2° under a scan rate of 2° per minute and generate structural information and degree of crystallinity.

Single crystal X-ray diffraction

Crystallographic data collection for the new FLZ polymorph was performed at 298 ± 2 K on a Bruker Super-Duo APEX II CCD diffractometer (Karlsruhe, Germany) using CuKα radiation (0.71073 Å). The data integration, Lorentz-polarization effects, and absorption corrections were performed using the CrysAlisPro (version 171.38.43b) software [34]. The structure was resolved by direct methods using the WingGX [35] and Olex2 [36] software packages, while the obtained model was refined using the full-matrix least-squares on F2 (SHELXTL–201539) [37]. The hydrogen atoms were placed in calculated positions and refined with fixed individual displacement parameters [Uiso(H) = 1.2Ueq or 1.5Ueq]. according to the riding model (C–H bond lengths of 0.97 Å and 0.96 Å, for methylene and methyl groups, respectively). The MERCURY programs (version 3.10.2) [38]. and ORTEP–3 were also used within the WinGX v1.70.0137 programs packages, to prepare the crystallographic information file (CIF) of the polymorph and its artwork representation for this publication. Finally, reported FLZ polymorphs were accessed from the Cambridge Structural Database (CSD) [39]. Table 1 presents the crystallographic data and structure refinement parameters of the new FLZ polymorph. All other refinement conditions including the bonds, torsions, and structure parameters can be accessed in the supporting information (SI). The CIF is deposited in the CCDC under code ***2163044*** (Fluconazole polymorph 10).

Thermogravimetric analysis (TGA)

The TGA of the samples was performed on a Netzsch TG 209 F1 analyzer (Germany), using an Al_2O_3 crucible pan under N_2(g) and a flow rate of 2 mL/min, heating rate conditions were set at 10 °C/min in the range of 25–325 °C. The samples were evaluated regarding the water/solvent content and degradation.

Differential scanning calorimetry (DSC)

This analysis was performed on a Shimadzu DSC-60 calorimeter (Kyoto, Japan). The samples (2 mg) were weighed and heated from 25 to 350 °C at a heating rate of 10 °C min^{-1} in a crimped sealed aluminium pan, using nitrogen as purge gas (50 mL/min). Data is processed using the Shimadzu TA-60 thermal software (version. 2.2).

Table 1
Crystallographic Data and Structure Refinement Parameters of FLZ Polymorph 10.

Identification code	FLZ Polymorph 10
CCDC depository number	*2163044*
Empirical formula	C_{13} H_{12} F_2 N_6 O
Formula weight	306.79
Temperature/K	273.15
Crystal system	Monoclinic
Space group	C2
a/Å	40.976(15)
b/Å	6.171(3)
c/Å	12.993(5)
α/°	90
β/°	107.24(3)
γ/°	90
Volume/$Å^3$	3138(2)
Z	8
ρ_{calc}g/cm^3	1.307
μ/mm^{-1}	0.896
F(000)	1284.0
Radiation	CuKα (λ = 1.54178)
2θ range for data collection/°	4.516 to 128.704
Index ranges	-47 ≤ h ≤ 47, -7 ≤ k ≤ 6, -14 ≤ l ≤ 15
Reflections collected	21110
Independent reflections	4987 [Rint = 0.0921, Rsigma = 0.0795].
Data/restraints/parameters	4987/1/400
Goodness–of–fit on F^2	0.972
Final R indexes [I>=2σ (I)].	R1 = 0.0604, wR2 = 0.1509
Final R indexes [all data].	R1 = 0.1257, wR2 = 0.1972
Largest diff. peak/hole / e $Å^{-3}$	0.24/-0.23

Stability Studies

The Stability check was performed at 75 % relative humidity (RH) under 40 °C for 2 weeks and monitored for up to 3 months to evaluate its phase transition and hygroscopicity. Thus, to maintain the RH, the samples were weighed and placed in a desiccator containing a saturated sodium chloride solution. The powder XRD of the sample is performed every 30 days for 3 months.

Solubility studies

The equilibrium solubility of the new polymorph was determined using UV-Vis 1800 Shimadzu spectrophotometer (Japan) with its absorbance determined at 270 nm using about 60–80 mg of sample in ultra-pure deionized water (10 mL) of pH = 7.0 (25.0 ± 0.1 °C), stirred for 30 min, and a UV-Vis calibration curve was developed to calculate the solubility. Herein, a few concentrations were attempted to obtain a clear saturated solution, and the solubility of the polymorph was obtained by diluting the saturated solution until it could be predicted by the calibration curve.

Results and discussion

Structural description of fluconazole polymorph 10

Fig. 1 presents the ORTEP-3 representation of the strong hydrogen bonds and crystal packing of the new FLZ polymorph 10, while the crystallographic data and structure refinement parameters are presented in Table 1. However, using Scheme 1, the major hydrogen bonds in the FLZ polymorph 10 are described in Table 2 (See S.I. for all other structural information).

Fluconazole polymorph 10

The polymorph crystallizes in the monoclinic space group C2 with two FLZ molecules in its asymmetric unit (Scheme 1). The FLZ molecules interact through strong O–H···N hydrogen bonds (O1-H1···N12 and O2-H2···N3) to form an infinite helix chain formation along the *a*-axis maintaining the 2_1-screw symmetry between the oxygen atom of the (–OH) hydroxyl group (bond donor) and the triazole nitrogen atom (bond acceptor) leading to a catemeric assembly along the [010]. direction. The structure is further connected and stabilized through sets of hydrogen bond interactions using different weak intramolecular interactions (C−H···X; X = N and F) such as C10−H10···N6 (3.319 Å) and C26−H26···N9 (3.306 Å) between adjacent triazole rings, while C−H···F interactions; C4−H4···F4 (3.278 Å), is observed between the neighboring phenyl rings of this polymorph. The interaction between adjacent methylene (−CH2−) groups i.e. CH···HC (2.372 Å) is observed alongside different infinite π-stacking interactions such as C25···N3 (3.087 Å), C10···N12 (3.073 Å), C9···C26 (3.098 Å), and C10···C25 (3.374 Å) are observed between three points on opposite triazole rings along the perpendicular *bc*-axis, and these contacts contribute to the infinite chains in the structure. The overall packing of this polymorph (Fig. 1b) shows two A and B (FLZ) molecules to form a dimer that involves the two O−H···N (O1-H1···N12 and O2-H2···N3) and

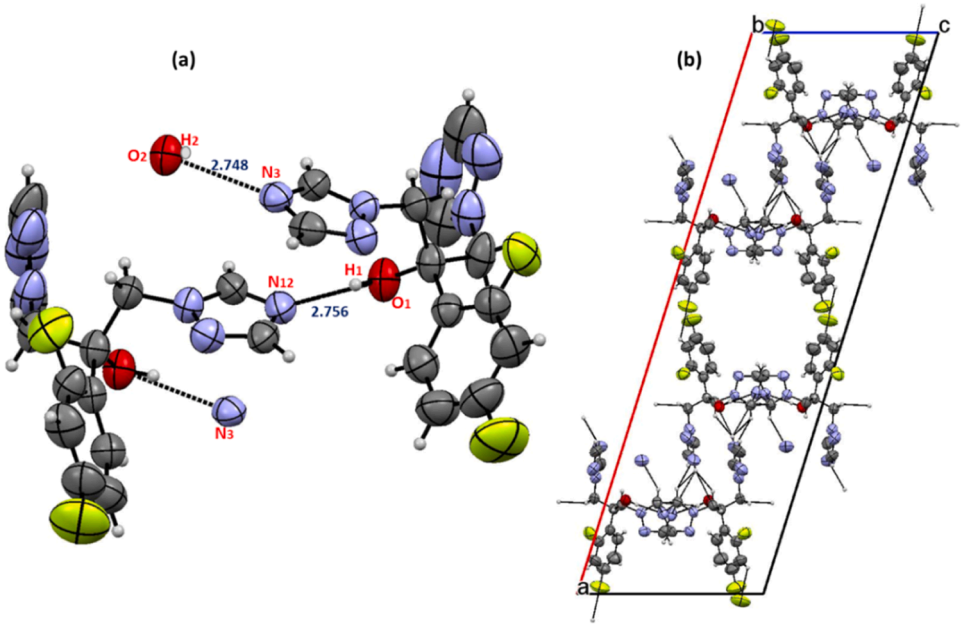

Fig. 1. (a) ORTEP-3 representation of the intermolecular O−H···N bonds, and (b) overall crystalline packing of FLZ polymorph 10. Thermal ellipsoids were drawn at a 50 % probability level.

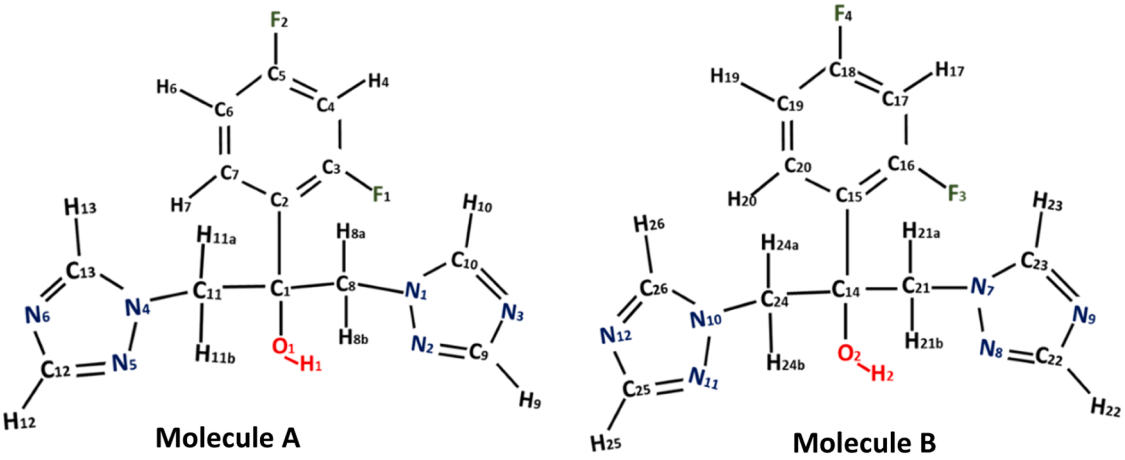

Scheme 1. Fluconazole Molecules with labelled atoms and molecule numbering.

Table 2
Intermolecular and Intramolecular Interactions in Fluconazole Polymorph 10.

D-H···A	D(D···A)Å	D(H···A)Å	d(H···A)/Å	∠D-H···A/°	Symmetry
O1−H1···N12	2.756	1.954	0.82	109.5	x, y, z
O2−H2···N3	2.748	1.959	0.82	120.17	-x -1, +y, 1-z
C4−H4···F4	3.278	2.612	0.93	129.6	-x, -1+y, 1-z,
C10−H10···N6	3.319	2.565	0.93	138.59	-1/2-x, -1/2+y, 1-z,
C26−H26···N9	3.306	2.569	0.93	136.58	1/2-x, -1/2+y, 2-z,

D-H···A; Hydrogen bond donor-acceptor interaction, D(D···A)Å; distances between the donor atoms, distance between hydrogen and acceptor atom D (H···A)Å, and bond generated angles; ∠D-H···A/°.

C−H···F (C4−H4···F4) hydrogen bonds. More so, the dimer extends through the π-stacking interactions and it makes this polymorph look a bit similar to polymorph 5 (*IVUQOF05*) [17]. Table 3 shows the comparison of the Crystallographic parameters of FLZ polymorph 10 with other FLZ forms and polymorphs obtained from the CCSD and literature.

Raman and FT-IR spectroscopic screening

Vibrational modes analyses

The Raman and FT-IR spectroscopy techniques were employed as complementary screening and characterization methods for the comparative study of the vibrational/absorption modes (active bands) of FLZ forms (II and III), including the FLZ hydrate that crystallizes spontaneously when FLZ is exposed to moisture or dissolved in solution. As shown in Fig. 2a-b, the sketched Raman and IR active bands and frequencies (shaded) of FLZ forms were developed to aid the screening for new FLZ polymorph [44]. Fig. 2a shows the Raman spectra of FLZ forms and it indicates the positions of important group vibrational modes (stretches and deformations) such as the C–C skeletal (371 cm^{-1}), -C=N str. (586, 1030 cm^{-1}), $–CH_2$, –OH, C–F of 2,4-difluorobenzyl, *ν*(C-N=C) and *ν*(C=N) of triazole, and C=C aromatic ring. (See S.I for tabulated vibrational and absorption modes of FLZ forms). It also shows the shaded chemical fingerprint regions that were monitored for inter- and intramolecular (non-covalent) interactions and bond contacts during the screening for the new FLZ polymorph. Fig. 2b presents the sketched FT-IR spectra from wavelength 4000 – 600 cm^{-1} showing the

Table 3
Comparison of the Crystallographic Parameters of FLZ polymorph 10 with selected FLZ forms/polymorphs.

Code Name	Space Group	Cell parameters
IVUQOF	$P\bar{1}$	a 7.49920(10) Å b 7.78690(10) Å c 11.9817(2) Å, α 84.9470(10)° β 84.6250 (10)° γ 75.8940(10)° [40]
IVUQOF01	P 21/n	a 6.6989(4) Å b 27.3867(19) Å c 15.2901(11) Å, α 90° β 90.319(3)° γ 90° [17]
IVUQOF02	P b c a	a 12.9282(9) Å b 6.0241(5) Å c 34.834(3) Å, α 90° β 90° γ 90° [17]
IVUQOF03	C 2/c	a 27.4726(9) Å b 10.9196(4) Å c 22.3424(12) Å, α 90° β 125.337(2)° γ 90° [17]
IVUQOF04	P b c a	a 10.9186(9) Å b 22.3367(18) Å c 22.3619(17) Å, α 90° β 90° γ 90° [17]
IVUQOF05	P b c a	a 12.8721(12) Å b 6.0216(5) Å c 34.770(3) Å, α 90° β 90° γ 90° [41]
IVUQOF06	$P\bar{1}$	a 7.51192(13) Å b 7.83226(16) Å c 12.0515(2) Å, α 84.7280(17)° β 84.7478(17)° γ 76.5371(18)° [42]
IVUQOF07	P b c a	a 12.9345(2) Å b 6.02210(10) Å c 34.8527(8) Å, α 90° β 90° γ 90° [43]
IVUQEV	P 21/c	a 6.04840(10) Å b 38.5004(6) Å c 12.9698(2) Å, α 90° β 90.2220(10)° γ 90° [40]
FLZ Polymorph 10	C2	a 40.976(15) Å b 6.171(3) Å c 12.993(5) Å, α 90° β 107.24(3)° γ 90°

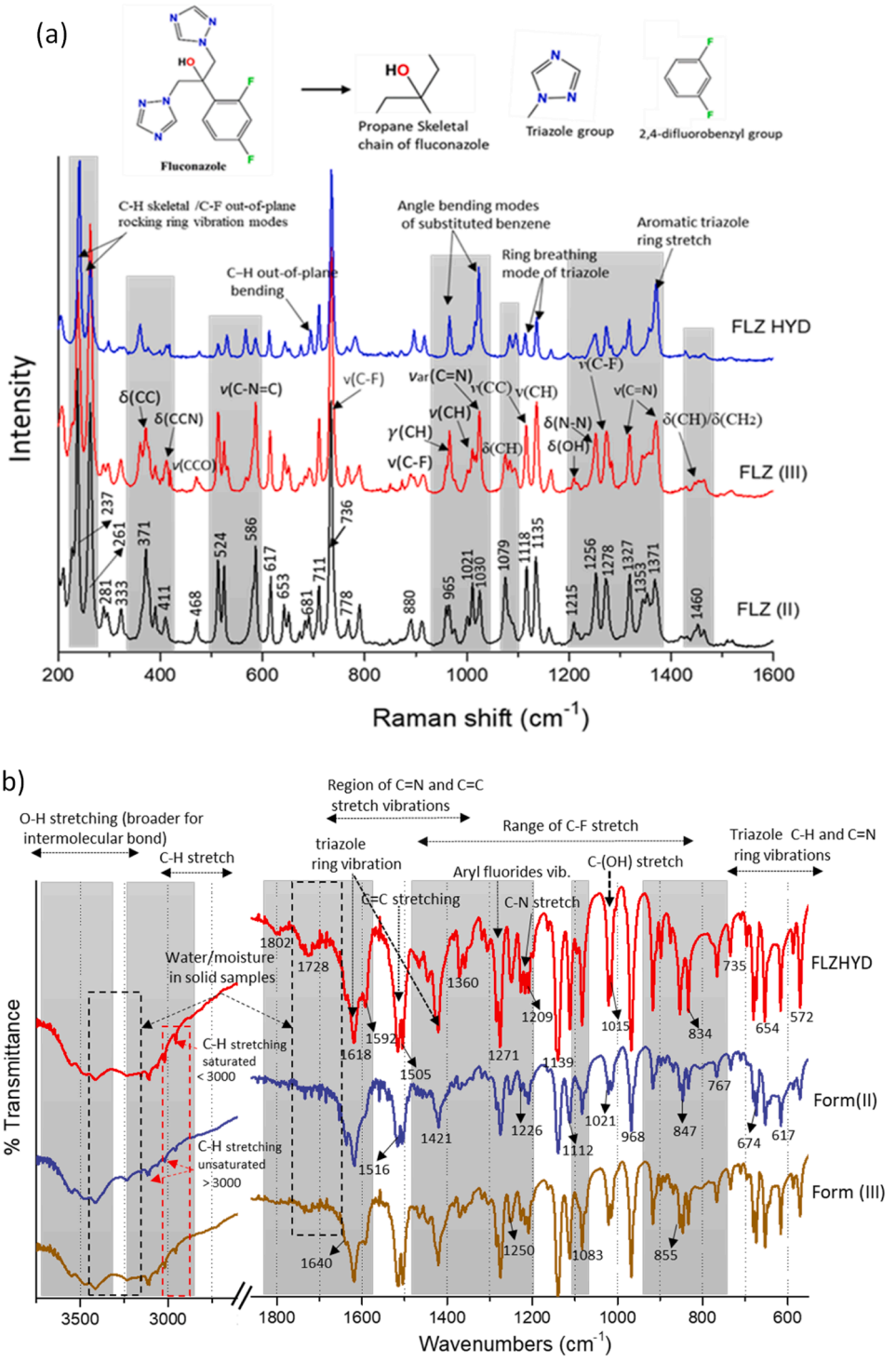

Fig. 2. (a) Raman and (b) FT-IR spectra showing peak positions and location of specific vibrational and absorption modes of fluconazole forms II, III and FLZ hydrate. Abbreviations: γ - out-of-plane bending, δ - in-plane bending, ν - stretching, and ar – aromatic.

active absorption bands for FLZ form II, III, and FLZ hydrate that aid the screening and characterization of inter/intramolecular interactions responsible for the formation of stable multicomponent forms and polymorphs of FLZ. The observed broad spectra peaks (shaded) are evidences that indicate the formation of strong hydrogen bonds like O–H···N, O–H···O, non-classical H-bonds C–H···N, C–H···F, and N^{+}–H···O^{-} in the multicomponent forms [20,21]. These observations were possible through PCA screening comparison of

absorption modes during *FLZ:coformer* cocrystallization. (See the S.I. for FLZ/coformers PCA screening).

Fig 3a-b shows the superimposed Raman and FT-IR spectra of different stoichiometric combinations of FLZ/MA (case study) as 1:2, 2:1, 3:1, 1:3, and FLZ forms. These spectra screening becomes a complex process due to the concomitant FLZ mixtures that hinder the

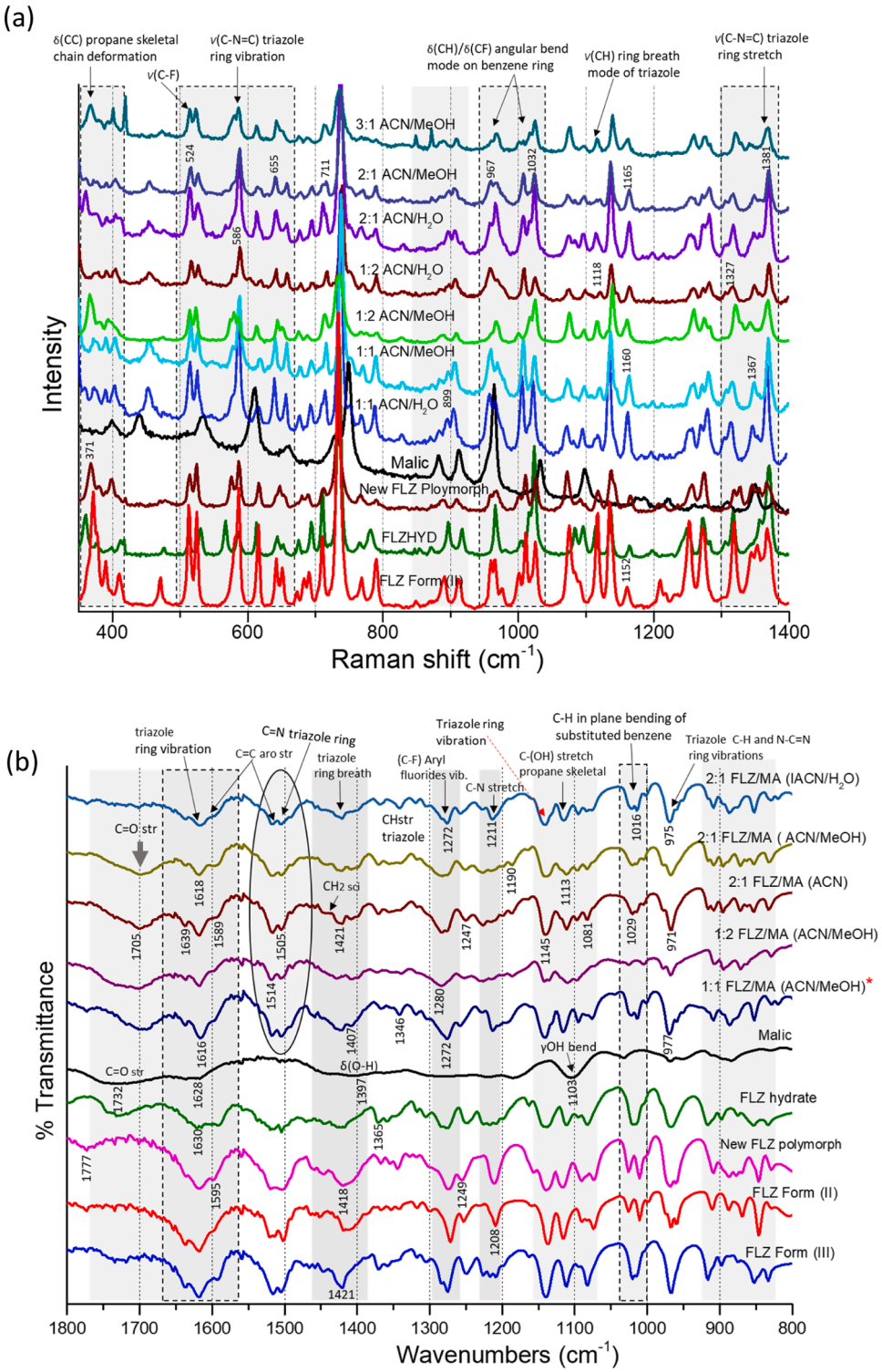

Fig. 3. Comparative analysis of the vibrational and absorption modes of FLZ forms and FLZ/MA combinations to differentiate the new FLZ polymorph; (a) Raman, and (b) FT-IR spectra.

conventional spectra superimposed screening, thus making it less efficient for differentiating homogenous spectra phases. Herein, the PCA is employed to decompose and screen spectra data of FLZ forms and reported *1:1 FLZ:coformers* (cocrystals/salt) by Owoyemi et al. [20]. The Raman data of important vibration modes such as the observed triazole ring vibrations are selected from spectra range between 200 and 1600 cm^{-1} (Fig. 3a) and decomposed to develop PCA models that predicted the new FLZ polymorph from samples synthesized below -4 °C in a refrigerator (lyophilization). In addition, the developed PCA–FT-IR model of absorption spectra data from FLZ/MA stoichiometric combinations (Fig. 3b) confirmed the new FLZ polymorph from the lyophilized samples synthesized below -4 °C. Therefore, combining PCA with the vibrational spectroscopic methods (Raman and IR characteristic group frequencies, Fig. 2) has effectively assisted in detecting, screening, and unveiling the reproducible synthesis route for producing the new FLZ polymorph 10 as a homogenous system.

PCA-Raman/FT-IR screening and vibrational modes analysis

The PCA decomposition of Raman and FT-IR spectra data of FLZ/MA combinations presented in Fig. 3a-b was performed using the sketched Raman and FT-IR vibrational and absorption modes/frequencies to select specific spectra regions and observe differences in the FLZ functionalities deformation. Herein, the shaded Raman spectra regions between 500 and 1400 cm^{-1} (Fig. 3a) that present intense FLZ groups vibrational modes, deformations, and the presence of new peaks are selected for PCA modeling of all the samples. Although the single crystal XRD characterization unveiled and confirmed the structure of the new FLZ polymorph, nevertheless, the PCA-Raman model in Fig. 4a is to be accredited for detecting the formation of this FLZ polymorph as a crystallized contaminant in the course to develop a computational screening method toward robust supramolecular syntheses routes to design homogenous FLZ multicomponent forms. Likewise, the developed PCA decomposition of FT-IR spectra data of FLZ forms and FLZ/coformer combinations taken from functional group region 1800 cm^{-1} to 800 cm^{-1} (Fig. 3b), confirmed the presence of new FLZ polymorph as presented in Fig. 4b. The PCA-Raman model (Fig. 4a) correlates FLZ form (II) and the new polymorph, such that the latter is easily assumed and mistaken for FLZ form (II) in the absence of single crystal XRD characterization. Interestingly, the PCA model differentiates and projects the FLZ forms (II, III, and hydrate) away from different stoichiometric FLZ/MA combinations and simplifies the selection of experimental conditions for robust crystallization of the new FLZ polymorph. In addition, the PCA FT-IR model with 84 % variance in Fig. 4b shows the differences within the score plots and projection of the new FLZ polymorph in a similar fashion to the PCA Raman model, thus signifying the advantage of employing both Raman and FT-IR spectroscopic techniques as complementary screening tools.

As mentioned earlier, the Raman/FT-IR spectra comparison of FLZ forms, new FLZ polymorph, and FLZ monohydrate present similar characteristic vibration/absorption bands at specific wavelength regions, thus making the screening for new polymorphic forms a complex task. Fig. 5a/c presents the results of the comparative Raman/FT-IR spectra studies on the aforementioned FLZ forms/polymorph, while Fig. 5b/d shows further PCA decomposition of spectra data to understand the useful information about homogeneity and transformation within the samples. The developed PCA-Raman model on vibrational data of functional groups that include the triazole ring ν(C-N=C) stretching at 586 cm^{-1}, 2,4-difluorobenzyl ν(C-F) stretching at 524 cm^{-1}, out-of-plane ring bending γ(CH) at 965 cm^{-1}, and benzyl ring stretching mode ν(C=C*ar.*) located at 1326 cm^{-1} aid the visual screening of the new FLZ polymorph in Fig. 5a-b. The PCA model with more than 86 % cumulative variance shows the visual projections of the FLZ forms and the new FLZ polymorph in a three-dimensional (3-D) PC1 vs. PC2 vs. PC3 fashion. The PC1/PC2 predicted the synthesis of a pure FLZ polymorph and its transformation to FLZ form (II) after three month exposure at room temperature. Likewise, Fig. 5c-d shows the comparison of FT-IR spectra of FLZ forms and polymorph, and the PCA model analysis of absorption modes data taken from wavelength 1800–800

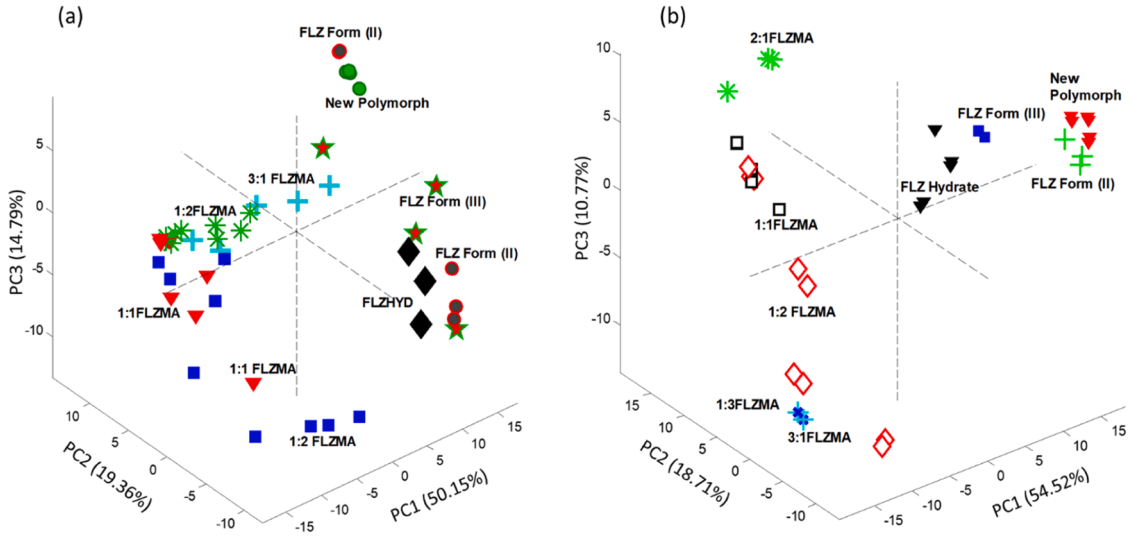

Fig. 4. PCA model of FLZ forms (II and III), FLZ hydrate, and FLZ/MA combinations: (a) PCA-Raman, and (b) PCA-FT-IR score plots.

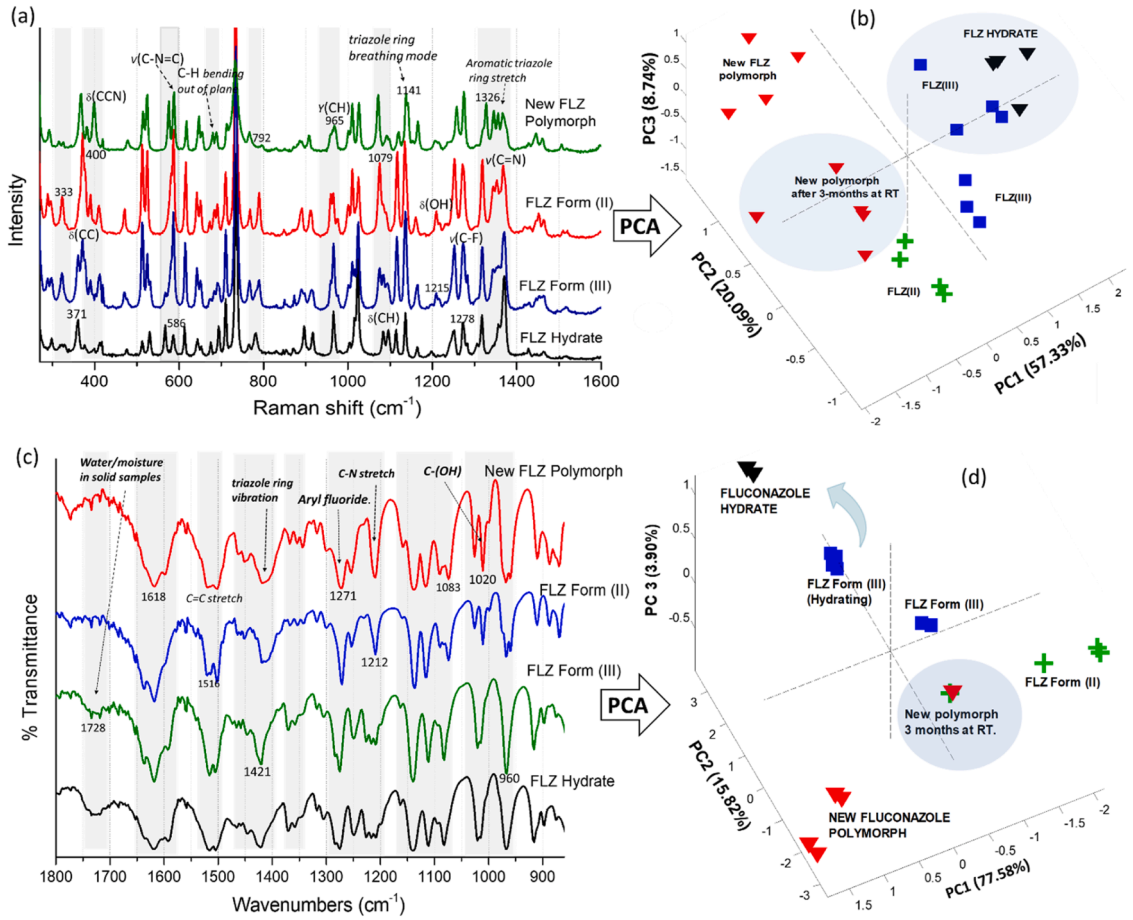

Fig. 5. Vibrational spectra comparison of FLZ forms (II and III), FLZ hydrate, and the new polymorph and their PCA modeling; (a/b) Raman spectra and their PCA model, and (c-d) FT-IR spectra and their PCA model.

cm^{-1}. As expected, the PC1 (77.58 %) vs. PC2 (15.82 %) shows the projection of the new FLZ polymorph and its transformation to FLZ form (II) after 3 months as predicted through observed correlation with FLZ form (II). However, the PCA models in Fig. 5 predict the projection of pure FLZ forms/polymorph with the tendency of the FLZ form (III) to transform into the hydrate form, and the propensity of the new FLZ polymorph to transform into FLZ form (II), thus making its screening, identification, and characterization very difficult. Although FLZ form (I) and FLZ monohydrate are the most stable FLZ forms, and the former is not included in the PCA models,

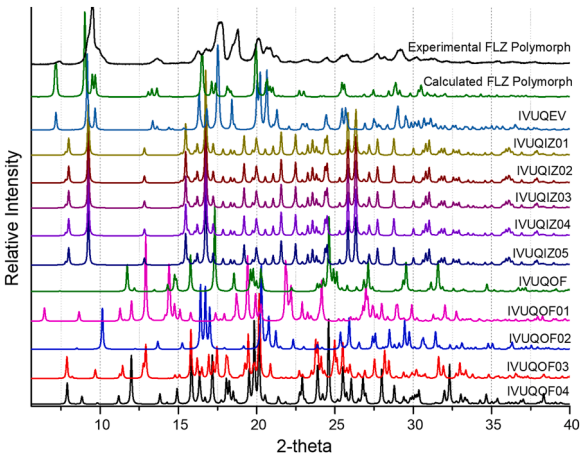

Fig. 6. Comparison of XRD patterns of the experimental, calculated of the new FLZ polymorph, and reported FLZ forms/polymorphs.

nevertheless, the new polymorph and FLZ form (II) may undergo polymorphic transformation into the stable form (I) under suitable conditions. Interestingly, studies on the kinetics of solid-state transformation of FLZ polymorph II (metastable form) to polymorph I (stable form) are comprehensively reported in the literature [45–47].

X-ray diffraction studies

The comparison of the experimental and calculated X-ray diffraction patterns for the new FLZ polymorph 10 shows good agreements of peaks, thus suggesting high purity, and further diffraction comparison with all reported FLZ forms/polymorphs taken from the range 5° to 40° (2θ) showed significant diffraction peaks differences as presented in Fig. 6. Herein, the plot of diffraction intensity as a function of 2θ values is the fingerprint characteristics and identity of crystalline materials that reflect the dimensions of unit cells and the arrangement of atoms or/and molecules. Therefore, each polymorphic form is distinguished based on the differences in diffraction peak positions and variation in peak intensities. Interestingly, the experimental and calculated diffraction patterns generated for the new FLZ polymorph match significantly at 7.3, 9.0, 9.6, 13.5, 16.5, 17.3,18.4, 19.8, 20.7, 21.5, 22.9, 24.3, 25.5, 26.6, 27.5, 28.4, 28.8, 29.2, 29.8, 30.5, 30.9, 32.0, 33.4 and 34.3 (2°θ). Although, this new monoclinic polymorph 10 (space group C2) presents few diffraction peaks similar to the triclinic FLZ monohydrate (*IVUQEV*, space group P 21/c). Nevertheless, differences in peak positions at 7.2, 8.7, doublet peak at 9.6 (2°θ), and other shifts in peak positions at 16.5, 17.3, and 19.8 (2°θ) differentiate the polymorph from the hydrate 7 days after synthesis and preparation. Therefore, the comparison of the polymorphs and their structural properties confirmed the uniqueness of the new FLZ polymorph as a metastable form that presents similarities with FLZ Form II.

As presented in Fig. 7, the stability of the new polymorph was determined between 1 and 3 months under 40 °C and 75 % relative humidity and indicates its readiness to spontaneously undergo phase transition (i.e. polymorphic transformation) into the FLZ form (II) rather than forming FLZ hydrate. However, the diffraction peaks in the shaded regions such as 7.6 - 10.2, 13.6, 15.3 – 22.0, 22.5, 24.3, 25.7, 27.8, and 29.0 (2°θ) confirmed the phase transition of the new polymorph into FLZ form II. However, the evidence of differences in their pattern is also observed with new peaks and peak shifts, especially at 9.3, 15.5, 23.7, 25.9, 29.3, and 37.5 (2°θ). Nevertheless, the new polymorph is expected to undergo polymorphic transformation into the stable form (I) under suitable conditions considering the similarities in their peaks at 10.2, 13.6, 15.5–22.0, (2°θ) (shaded diffraction region, Fig. 7) observed after 90 days under 40 °C and 75 % RH. Finally, it is expected that FLZ will spontaneously transform into the hydrate form when subjected to a moisture or dilution condition and this discrepancy is observed with the physical manifestation of FLZ needle crystals observable as a broader peak band in the IR spectra at 3000cm^{-1}.

Thermal analysis and characterization (DSC/TGA)

Fig 8a-b shows the generated DSC and TGA thermal analysis results for the new FLZ polymorph to determine/confirm its purity, composition, melting point, etc. The DSC analysis result graph of the polymorph (Fig. 8a) shows a sharp endothermic peak that indicates the melting point at 139.90°C, an onset, and endset melting temperatures at 137.71°C and 142.91°C respectively. However, the small broad peak at 73.01 °C with an onset (53.23 °C) and endset (82.11 °C) temperatures is assumed to have occurred due to moisture or equipment over-sensitivity. Thus, this result confirmed the FLZ polymorph as an anhydrous form. As expected, polymorphs of a compound present very similar physical properties like melting point. Hence, according to the literature, the anhydrous forms I, II, and III present melting points at 139.7 °C, 138.2 °C, and 139.2 °C, respectively, which are closer to that of the new polymorph. These figures slightly differ with about ±2.00 °C for all polymorphic forms of FLZ reported in the literature due to environmental and equipment over-sensitivity. Fig. 8b shows the TGA result of the new FLZ polymorph taken at a temperature range between 40 and 400 °C to determine its composition and thermal stability. As observed through the TGA curve, the new polymorph indicates no weight

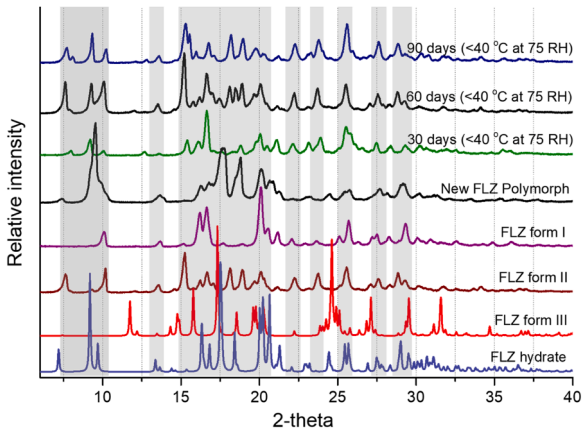

Fig. 7. XRD stability studies of new FLZ polymorph between 30 and 90 days under 40 °C and 75 % RH and comparison with FLZ forms I, II, III, and FLZ hydrate.

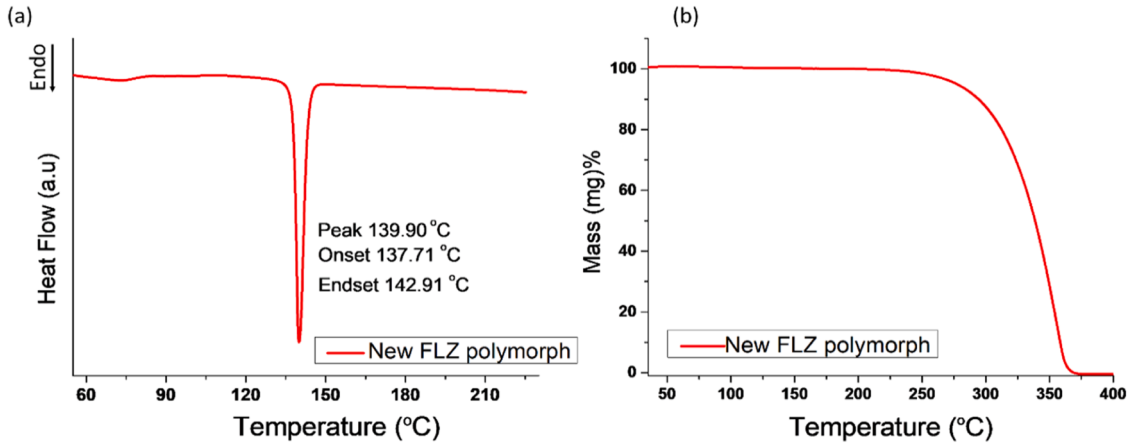

Fig. 8. DSC and TGA of the new FLZ polymorph

loss on uniform heating from 40 to 280 °C (Tg_{onset} at 310 °C) with a uniform decomposition (Tg_{offset} at 368 °C) to 400 °C. However, the small broad peak at 73.01 °C in the DSC result is confirmed to occur due to equipment over-sensitivity rather than water loss due to dehydration. Finally, the DSC and TGA further confirmed the novelty and stability of the new FLZ polymorph as detected by the Raman/FT-IR- PCA models and XRD analyses.

Solubility of new FLZ polymorph

The aqueous solubility of the new FLZ polymorph 10 was determined by dissolving about 60 mg of its crystal sample in 10 mL of ultra-pure deionized water (pH = 7.0 at 25.0 ± 0.1 °C). The absorbance was determined at 270 nm and was used to calculate (predict) the equilibrium solubility of the polymorph from the linear relationship between plots of known concentrations *vs* absorbance. However, the solubility result obtained for the FLZ polymorph 10 after a series of repeated trials is 3.97 mg/mL. Thus, this calculated solubility is considered to agree with our expected value considering that, FLZ forms can easily hydrate into the more stable and less soluble FLZ monohydrate (solubility 3.56 mg/mL) as presented in Table 4.

Conclusion

In this report, the crystallization experiment using FLZ/MA stoichiometric combinations was selected to demonstrate the Raman and FT-IR spectra screening and detection of the new FLZ polymorph 10 through PCA modeling of acquired spectra data. Vibrational spectroscopy is an established characterization tool for monitoring, detecting, and investigating the molecular properties of materials through spectra analysis (comparison). However, the conventional screening (spectra superimpose) becomes confusing/complicated to differentiate complex spectra. Thus, a judicious combination of principal component analysis (PCA) with vibrational spectroscopy as an unbiased screening and characterization method for detecting differences in the supramolecular interactions through vibrational modes analysis and comparison of functional groups vibrations is thoroughly presented in this paper. The PCA models effectively detect trends within crystallized samples (score plots) and aid the selection of desired robust and homogenous synthesis routes to produce the new FLZ polymorph 10. According to its generated crystallographic parameters the *chemical formula moiety* calculated were 0.5(C_{13} H_{13} F_2 N_6 O) and 0.5(C_{13} H_{12} F_2 N_6 O) with a *chemical formula sum* as 'C_{13} $H_{12.5}$ F_2 N_6 O' (306.79 g/mol) due to the isotopic differences of protium [1H]. and deuterium [2H].. However, a [3H].Fluconazole with the chemical formula C_{13} H_{12} F_2 N_6 O (*Mw* = 308.28 g/mol) was reported and patented [41,49]. The polymorph 10 is unveiled as a monoclinic of the space group C2, the phase identification and transition are limited to powder X-ray diffraction analysis after 90 days under 40 °C and 75 % RH, while thermal analysis techniques (TGA and DSC) provide its important structural properties such as its melting point at 139.90 °C and confirmed its stability at ambient temperature.

Associated content

Supplementary Information (S.I.) Calculated X-ray powder diffractogram files of the FLZ polymorph crystalline structures reported on the CSD, accessed via the Mercury program, for comparison. Refcodes: CCDC *2163044*. These data can be obtained free via www.ccdc.cam.ac.uk/data_request/cif, by emailing data_request@ccdc.cam.ac.uk, or by contacting The Cambridge Crystallographic Data Centre, 12 Union Road, Cambridge CB2 1EZ, UK; fax: +44 1223 336033.

CRediT authorship contribution statement

Bolaji C. Dayo Owoyemi: Conceptualization, Methodology, Validation, Investigation, Data curation, Supervision, Writing –

Table 4
Aqueous Equilibrium Solubility of FLZ Forms and reported polymorphs in Comparison with the new polymorph 10.

Fluconazole forms	Molar weight (g/mol)	Water solubility mg/mL
FLZ Form I	306.27	4.29 [16], (4.96–5.02) [48]
FLZ Form II	306.27	4.61 [16], (6.59–7.88) [48]
FLZ Form III	306.27	5.03 [23]
FLZ monohydrate	324.29	3.56 [16], 4.21 [48]
New FLZ Polymorph	306.79	3.97

original draft, Project administration, Funding acquisition. **Cecilia C.P. da Silva:** Methodology, Validation, Investigation, Writing – review & editing. **Amos O. Akinyemi:** Software, Investigation, Data curation, Writing – review & editing. **Banky O. Amuwaolorun:** Software, Investigation, Writing – review & editing. **Roxana Lili Roque-Flores:** Investigation, Writing – review & editing. **Gabriel Lima Barros de Araújo:** Methodology, Validation, Investigation, Writing – review & editing. **Javier Ellena:** Methodology, Validation, Investigation, Writing – review & editing. **Renato L. Carneiro:** Methodology, Validation, Investigation, Writing – review & editing.

Declaration of Competing Interest

The authors declare that they have no known competing financial interests or personal relationships that could have appeared to influence the work reported in this paper.

References

[1] V. Kumar, V. Bansal, A. Madhavan, M. Kumar, R. Sindhu, M.K. Awasthi, P. Binod, S. Saran, Active pharmaceutical ingredient (API) chemicals: a critical review of current biotechnological approaches, Bioengineered 13 (2) (2022) 4309–4327.
[2] J. Chakraborty, M. Subash, B.N. Thorat, Drying induced polymorphic transformation of pharmaceutical ingredients: a critical review of recent progresses and challenges, Dry. Technol. (2021) 1–19.
[3] J. Lu, S. Rohani, Polymorphism and crystallization of active pharmaceutical ingredients (APIs), Curr. Med. Chem. 16 (7) (2009) 884–905.
[4] M. Saifee, N. Inamda, D. Dhamecha, A. Rathi, Drug polymorphism: a review, Int. J. Health Res. 2 (4) (2009).
[5] R. Tandon, N. Tandon, N. Gupta, R. Gupta, Art of synthesis of desired polymorphs: a review, Asian J. Chem. 30 (2018) 5–14.
[6] S. Piqueras, L. Duponchel, R. Tauler, A. De Juan, Monitoring polymorphic transformations by using *in situ* Raman hyperspectral imaging and image multiset analysis, Anal. Chim. Acta 819 (2014) 15–25.
[7] S. Fateixa, H.I. Nogueira, T. Trindade, Carbamazepine polymorphism: A re-visitation using Raman imaging, Int. J. Pharm. 617 (2022), 121632.
[8] V. Bhavana, R.B. Chavan, M.C. Mannava, A. Nangia, N.R. Shastri, Quantification of niclosamide polymorphic forms–a comparative study by Raman, NIR and MIR using chemometric techniques, Talanta 199 (2019) 679–688.
[9] K. Richardson, K. Cooper, M. Marriott, M. Tarbit, F. Troke, P. Whittle, Discovery of fluconazole, a novel antifungal agent, Rev. Infect. Dis. 12 (Supplement_3) (1990) S267–S271.
[10] K. Richardson, The discovery of fluconazole, Contemp. Org. Synth. 3 (2) (1996) 125–132.
[11] M. Zervos, F. Meunier, Fluconazole (Diflucan®): a review, Int. J. Antimicrob. Agents 3 (3) (1993) 147–170.
[12] X. Gu, W. Jiang, Characterization of polymorphic forms of fluconazole using Fourier transform Raman spectroscopy, J. Pharm. Sci. 84 (12) (1995) 1438–1441.
[13] Y.L. Yang, Y.A. Ho, H.H. Cheng, M. Ho, H.J. Lo, Susceptibilities of Candida species to amphotericin B and fluconazole: the emergence of fluconazole resistance in Candida tropicalis, Infection Control & Hospital Epidemiology 25 (1) (2004) 60–64.
[14] A.K. Dash, W.F. Elmquist, Fluconazole. Analytical profiles of Drug Substances and Excipients, Elsevier Inc, 2001, pp. 67–113.
[15] H.J. Park, M.S. Kim, S. Lee, J.S. Kim, J.S. Woo, J.S. Park, S.J. Hwang, Recrystallization of fluconazole using the supercritical antisolvent (SAS) process, Int. J. Pharm. 328 (2) (2007) 152–160.
[16] K.A. Alkhamis, A.A. Obaidat, A.F. Nuseirat, Solid-state characterization of fluconazole, Pharm. Dev. Technol. 7 (4) (2002) 491–503.
[17] M. Karanam, S. Dev, A.R. Choudhury, New polymorphs of fluconazole: results from cocrystallization experiments, Cryst. Growth Des. 12 (1) (2012) 240–252.
[18] R.G. Gonnade, E. Sangtani, Polymorphs and cocrystals: a comparative analysis, J. Indian Inst. Sci. 97 (2) (2017) 193–226.
[19] S. Blokhina, M. Ol'khovich, A. Sharapova, G. Perlovich, Experimental investigation of fluconazole: equilibrium solubility and sublimation, J. Chem. Thermodyn. 151 (2020), 106243.
[20] B.C. Dayo Owoyemi, C.C. da Silva, M.S. Souza, L.F. Diniz, J. Ellena, R.L. Carneiro, Fluconazole: synthesis and structural characterization of four new pharmaceutical cocrystal forms, Cryst. Growth Des. 19 (2) (2019) 648–657.
[21] B.C.D. Owoyemi, C.C. da Silva, L.F. Diniz, M.S. Souza, J. Ellena, R.L. Carneiro, Fluconazolium oxalate: synthesis and structural characterization of a highly soluble crystalline form, CrystEngComm 21 (7) (2019) 1114–1121.
[22] M. Nowak, A.J. Dyba, J. Janczak, A. Morritt, L. Fábián, B.e. Karolewicz, Y.Z. Khimyak, D.E. Braun, K.P. Nartowski, Directing crystallization outcomes of conformationally flexible molecules: polymorphs, solvates, and desolvation pathways of fluconazole, Mol. Pharm. (2022).
[23] N. Charoo, R. Cristofoletti, A. Graham, P. Lartey, B. Abrahamsson, D. Groot, S. Kopp, P. Langguth, J. Polli, V.P. Shah, Biowaiver monograph for immediate-release solid oral dosage forms: fluconazole, J. Pharm. Sci. 103 (12) (2014) 3843–3858.
[24] A.O. Surov, A.P. Voronin, N.A. Vasilev, A.V. Churakov, G.L. Perlovich, Cocrystals of fluconazole with aromatic carboxylic acids: competition between anhydrous and hydrated solid forms, Cryst. Growth Des. 20 (2) (2019) 1218–1228.
[25] J. Kastelic, Z. Hodnik, P. Šket, J. Plavec, N. Lah, I. Leban, M. Pajk, O. Planinšek, D. Kikelj, Fluconazole cocrystals with dicarboxylic acids, Cryst. Growth Des. 10 (11) (2010) 4943–4953.
[26] H.G. Brittain, Cocrystal systems of pharmaceutical interest: 2010, Cryst. Growth Des. 12 (2) (2012) 1046–1054.
[27] N.L. Calvo, R.M. Maggio, T.S. Kaufman, Chemometrics-assisted solid-state characterization of pharmaceutically relevant materials. Polymorphic substances, J. Pharm. Biomed. Anal. 147 (2018) 518–537.
[28] S. Karamizadeh, S.M. Abdullah, A.A. Manaf, M. Zamani, A. Hooman, An overview of principal component analysis, J. Signal Inf. Process. 4 (2020).
[29] S.P. Mishra, U. Sarkar, S. Taraphder, S. Datta, D. Swain, R. Saikhom, S. Panda, M. Laishram, Multivariate statistical data analysis-principal component analysis (PCA), Int. J. Livest. Res. 7 (5) (2017) 60–78.
[30] L. Pan, P. Zhang, C. Daengngam, S. Peng, M. Chongcheawchamnan, A review of artificial intelligence methods combined with Raman spectroscopy to identify the composition of substances, J. Raman Spectrosc. 53 (1) (2022) 6–19.
[31] P. Guccione, M. Lopresti, M. Milanesio, R. Caliandro, Multivariate analysis applications in x-ray diffraction, Crystal 11 (1) (2020) 12.
[32] N. Chieng, T. Rades, J. Aaltonen, An overview of recent studies on the analysis of pharmaceutical polymorphs, J. Pharm. Biomed. Anal. 55 (4) (2011) 618–644.
[33] M. Rodrigues, J. Lopes, M. Sarraguça, Vibrational spectroscopy for cocrystals screening. A comparative study, Molecules 23 (12) (2018) 3263.

[34] P. CrysAlis, Agilent Technologies: Yarnton, Oxfordshire, England, 2010.
[35] L.J. Farrugia, WinGX and ORTEP for Windows: an update, J. Appl. Crystallogr. 45 (4) (2012) 849–854.
[36] O.V. Dolomanov, L.J. Bourhis, R.J. Gildea, J.A. Howard, H. Puschmann, OLEX2: a complete structure solution, refinement and analysis program, J. Appl. Crystallogr. 42 (2) (2009) 339–341.
[37] G.M. Sheldrick. Program for the refinement of crystal structures, Shelx l97, 1997, https://doi.org/10.1107/S0108767307043930.
[38] C.F. Macrae, I.J. Bruno, J.A. Chisholm, P.R. Edgington, P. McCabe, E. Pidcock, L. Rodriguez-Monge, R. Taylor, J. Streek, P.A. Wood, Mercury CSD 2.0–new features for the visualization and investigation of crystal structures, J. Appl. Crystallogr. 41 (2) (2008) 466–470.
[39] F.H. Allen, The Cambridge structural database: a quarter of a million crystal structures and rising, Acta Crystallogr. Sect. B Struct. Sci. 58 (3) (2002) 380–388.
[40] M.R. Caira, K.A. Alkhamis, R.M. Obaidat, Preparation and crystal characterization of a polymorph, a monohydrate, and an ethyl acetate solvate of the antifungal fluconazole, J. Pharm. Sci. 93 (3) (2004) 601–611.
[41] https://pubchem.ncbi.nlm.nih.gov/compound/3H_- Fluconazole 2023. [https://pubchem.ncbi.nlm.nih.gov/compound/46906107].
[42] P.A. Basford, K.R. Back, M. Cram, R. Docherty, R.J. Davey, A.J. Cruz-Cabeza, Impact of crystal structure and molecular conformation on the hydration kinetics of fluconazole, Cryst. Growth Des. 19 (12) (2019) 7193–7205.
[43] X. Ou, X. Li, H. Rong, L. Yu, M. Lu, A general method for cultivating single crystals from melt microdroplets, Chem. Commun. 56 (69) (2020) 9950–9953.
[44] G. Socrates, Infrared and Raman Characteristic Group Frequencies: Tables and Charts, John Wiley & Sons, 2004.
[45] S. Desai, M. Shaikh, S. Dharwadkar, Thermoanalytical study of polymorphic transformation in fluconazole drug, Thermochim. Acta 399 (1-2) (2003) 81–89.
[46] R.M. Obaidat, K.A. Alkhamis, M.S. Salem, Determination of factors affecting kinetics of solid-state transformation of fluconazole polymorph II to polymorph I using diffuse reflectance Fourier transform spectroscopy, Drug Dev. Ind. Pharm. 36 (5) (2010) 570–580.
[47] E.A. Gorkovenko, S.E. Kichanov, D.P. Kozlenko, A.V. Belushkin, J. Wąsicki, W. Nawrocik, J. Mielcarek, L.S. Dubrovinsky, C. Lathe, B.N. Savenko, The pressure-induced polymorphic transformations in fluconazole, J. Pharm. Sci. 104 (12) (2015) 4164–4169.
[48] H.J. Park, M.S. Kim, J.S. Kim, W. Cho, J. Park, K.H. Cha, Y.S. Kang, S.J. Hwang, Solid-state carbon NMR characterization and investigation of intrinsic dissolution behavior of fluconazole polymorphs, anhydrate forms I and II, Chem. Pharm. Bull. 58 (9) (2010) 1243–1247.
[49] https://www.ebi.ac.uk/chembl/compound_report_card/CHEMBL1163001/ 2023.